GMe Forum 2003

Abstracts of the Poster Presentations

Vienna University of Technology
April 10 and 11, 2003

Society for Microelectronics
Vienna, 2003

Society for Microelectronics
c/o Institute of Industrial Electronics and Material Science
Vienna University of Technology
Gusshausstraße 27–29/366
A-1040 Vienna, Austria

Opto-Electronics:

S. ANDERS et al. (TU Wien): "*Electrically Pumped Quantum Cascade Ring Lasers*"

A. ANDREEV et al. (JKU Linz): "*Anisotropic Optoelectronic Properties of Self-Assembled Nano-Wires of Para-Sexiphenyl Grown by Hot Wall Epitaxy*"

J. DARMO et al. (TU Wien): "*New Generation of Photoconductive Terahertz Emitters*"

G. KOCHER-OBERLEHNER et al. (JKU Linz): "*Enhanced Luminescence of Erbium Doped Silicon Due to Hydrogen*"

T. MÜLLER et al. (TU Wien): "*Time-Resolved Measurement of Intersubband Population Dynamics*"

F.F. SCHREY et al. (TU Wien): "*Dynamics between Electronic Levels in InAs Quantum Dots*"

T. SCHWARZL et al. (JKU Linz): "*Comparison of MBE Grown IV–VI Microcavity Lasers for the Mid-Infrared with Active Regions of Different Dimensionality*"

IV-VI Semiconductors:

A. HALLBAUER et al. (JKU Linz): "*Molecular Beam Epitaxy of $PbSe_{1-x}Te_x$ for Strain Engineering in IV-VI Semiconductor Heterostructures*"

A. RAAB et al. (JKU Linz): "*Intermixing and Shape Transitions of PbSe Quantum Dots During Overgrowth*"

Silicon and SiGe:

H. LICHTENBERGER et al. (JKU Linz): "*Transient-Enhanced Surface Diffusion on Natural-Oxide-Covered Si(001) Templates During Vacuum Annealing*"

M. MÜHLBERGER et al. (JKU Linz): "*Growth Instabilities in Si/SiGe Homo- and Heteroepitaxy*"

M. MÜHLBERGER et al. (JKU Linz): "*High-mobility Strained Si for Spintronics Applications*"

Z. ZHONG et al. (JKU Linz): "*Laterally Ordered Ge Islands on the Pre-Patterned Si (001) Substrates*"

Direct Write Processes:

W. BREZNA et al. (TU Wien): "*Focused Ion Beam Induced Damage in Silicon Investigated with Scanning Capacitance Microscopy*"

A. LUGSTEIN et al. (TU Wien): "*Post-Process CMOS Channel Profile Tailoring with Focused Ion Beams*"

H.D. WANZENBOECK et al. (TU Wien): "*Deposition Mechanism of Direct-Write Processes — An Application-Oriented Approach to Custom-Tailored Material Properties*"

Insulating Films:

S. HARASEK et al. (TU Wien): "*Zirconium Dioxide Thin Films for Microelectronics Deposited by Metal Organic Chemical Vapor Deposition*"

Transport Phenomena:

M. KAST et al. (TU Wien): "*Transport through Wannier-Stark States in Biased Finite Superlattices*"

Sensors:

F. KEPLINGER et al. (TU Wien): "*Simulated and Measured Characteristic of a Micromachined Cantilever Sensor*"

J.H. NIEUWENHUIS et al. (TU Wien): "*Novel Flow-Cell To Create A Sheath Flow With Adaptable Sample Flow Dimensions*"

P. SVASEK et al. (TU Wien): "*Micromachined Mixing Device for FTIR-Spectroscopy*"

Electrically Pumped Quantum Cascade Ring Lasers

S. Anders, P. Schwaha, T. Roch, W. Schrenk, and G. Strasser
Inst. für Festkörperelektronik
Technische Universität Wien, A-1040 Wien

Quantum cascade lasers are unipolar heterostructures with several tens of light-emitting cascades in series. Both the InGaAs/InAlAs/InP and the GaAs/AlGaAs material systems are well established. The emission wavelength can be tailored by the thickness of the well and barrier layers and ranges from the mid-infrared to the far-infrared. This emission range is useful for example for chemical analysis, environmental sensing, and free space communication.

The lasers were grown by standard solid source molecular beam epitaxy. They consist of typically 30 – 50 cascades, resulting in up to 1500 layers and a total thickness of up to 15 microns per growth. The good quality of an AlAs/GaAs superlattice structure is shown by x-ray analysis.

Quantum cascade lasers are mostly processed as ridge waveguides. Apart from this geometry, circular and quadrupolar-shaped waveguides have been explored. Such designs take advantage of the low losses for total internal reflection of the propagating light. Sufficiently smooth and perpendicular sidewalls can be obtained by reactive ion etching of the cavity. Recently, a comparison between Fabry-Perot, distributed feedback, and microcylinder-shaped cavities has shown the satisfying performance of the microcylinders.

As a step further, we fabricated ring lasers. Because the whispering gallery modes in circular geometries travel close to the perimeter of the cavity, it is expected that a microcylinder with a sufficiently small hole in the center shows properties equal to a conventional microcylinder. By fabricating ring lasers with fixed outer diameters of 200 to 400 µm and varying inner diameters, we explored the effect of the hole on the whispering gallery modes. We found that even for an inner diameter of only ¼ of the outer diameter, the lasing threshold and the temperature performance degrade somewhat (although room temperature operation is still possible for some devices). Furthermore, the modes are not evenly spaced as is expected for whispering gallery modes. This demonstrates the influence of the central region on the operation of circular lasers.

To elucidate how the current distribution (which is, because of the comparable size of the bonding pads and the width of the rings, necessarily inhomogeneous) affects the operation of the lasers, we bonded microcylinder and ring lasers at various positions and with differing numbers of bonding wires. Preliminary results indicate that the placement of the bonding pads is indeed critical to achieve a low threshold and a high light power output.

Future work may include the mapping of the temperature distribution (and hence the current distribution) of ring lasers. This could yield more insight into the influence of the geometry on the lasing modes so that an optimized micro-geometry can be designed.

Anisotropic Optoelectronic Properties of Self-Assembled Nano-Wires of Para-Sexiphenyl Grown by Hot Wall Epitaxy

A. Andreev[1], H. Sitter[1], N. S. Sariciftci[2], A. Kadashchuk[3], C. Winder[2], R. Resel[4], D.-M. Smilgies[5]

[1] Institute for Semiconductor and Solid State Physics, Johannes Kepler University Linz, Austria

[2] Linz Institute for Organic Solar Cells (LIOS), Physical Chemistry, Johannes Kepler University Linz, Austria

[3] Institute of Physics, National Academy of Sciences of Ukraine, Kiev, Ukraine

[4] Institute of Solid State Physics, Graz University of Technology, Austria

[5] CHESS G-line, Cornell University, Ithaca NY 14853, USA

Conjugated oligomers like oligophenylenes or oligothiophenes show potential for different optoelectronic applications. We focus on the study of epitaxially grown structures based on the organic semiconductor para-sexiphenyl (PSP) grown by Hot Wall Epitaxy (HWE). This technique allows growing epilayers close to thermodynamic equilibrium, which is essential in the case of van der Waals epitaxy of fullerenes and oligophenylenes [1], [2].

Para-sexiphenyl (PSP) molecules perform self-organization during growth by HWE on mica substrates [2]. As a consequence the epilayers show highly ordered needle-like crystalline structures in nanometer dimensions with dichroic ratios in photoluminescence of up to 14 [2], [3]. In this work we use atomic force microscopy, X-ray diffraction (XRD) and optical spectroscopy to study the deposition process of these structures in detail, in order to find the parameters controlling their morphology and crystalline quality.

It is shown that the substrate temperature is the most decisive parameter for the morphology of the films and therewith for the growth mode. Furthermore, XRD and optical investigations confirmed the high degree of anisotropic epitaxial order within the grown films.

We investigated also the growth of PSP on other layered crystalline substrates like $MoSe_2$ and GeS, which are electrically conductive and therefore interesting as substrates for opto-electronic applications. We were able to demonstrate that the “Van der Waals epitaxy” on $MoSe_2$ and GeS results in self-ordered anisotropic structures of PSP comparable to those on mica.

The first attempts to use the advantages of the HWE technique for device applications like OLED’s and organic solar cells will be also discussed.

References:

[1] D. Stifter, H. Sitter, Appl. Phys. Lett. **66(6)**, 679 (1995).

[2] A. Andreev, G. Matt, C.J. Brabec, H. Sitter, D. Badt, H. Seyringer, N. S. Sariciftci, Adv. Mat. **12(9)**, 629 (2000).

[3] H. Plank, R. Resel, S. Purger, J. Keckes, A. Thierry, B. Lotz, A. Andreev, N. S. Sariciftci, H. Sitter, Phys. Rev. B **64**, 235423 (2001).

New Generation of Photoconductive Terahertz Emitters

J. Darmo, T. Roch, G. Strasser, T. Müller, and K. Unterrainer
Institute of Solid State Electronics, Vienna University of Technology,
Floragasse 7, A-1040 Vienna, Austria

The generation of few-cycle Terahertz radiation into the free space from a biased photoconductive gap is known for more than a decade. Since then, many attempts were presented to increase the generated THz power without compromising the radiation bandwidth.

In this contribution, we report on a low-temperature-grown GaAs (LT GaAs) based photoconductive THz emitter integrated with a Bragg mirror. This design improves the generator's THz output power by about one order of magnitude. The optical resonance and the confinement of the photogenerated carriers in the high electric field region of LT GaAs layers are responsible for the observed enhancement of the THz emission. Such structure was already successfully applied for THz generation in a fs-laser cavity.

In addition, we have focused on the optimization of the growth temperature of the LT GaAs layer with respect to maximum photoresponse of the material and maximum breakdown field. It is known that annealed LT GaAs changes its properties (resistivity, carrier lifetime) with the growth temperature. Our experiences from THz emission experiments suggest a decreasing THz power output from emitters when the growth temperature is lowered. Therefore, we designed and tested a multilayer LT GaAs structure to increase the performance of the THz emitters.

Finally, we present preliminary results of imaging in the Terahertz frequency range using new generation emitters.

Enhanced luminescence of Erbium doped Silicon due to Hydrogen

G. Kocher-Oberlehner[1], W. Jantsch[1], L. Palmetshofer, A. Ulyashin[2]
[1] University of Linz, Altenbergerstr. 69, 4040 Linz
[2] Univ. of Hagen, Haldener Str. 182, PO Box 940, D-58084 Hagen, Germany

Erbium emits light at a wavelength of 1.54 µm due to an intrashell transition within the 4 f shell. This wavelength appears to be ideal for fibre optical communication systems because of its coincidence with the absorption minimum in conventional fibres. After intense investigations of co-doping of Si with Er and light elements, it was found that in particular O leads to high luminescence yields at low temperatures [1], [2].

Hydrogen plasma treatment is widely used in semiconductor technology for the gettering and passivation of residual defects. Hydrogen is known to enhance the oxygen diffusion and to form complexes with oxygen at defects in silicon [3]. We expected therefore a positive effect of hydrogen on the formation of Er-O complexes and precipitates which are necessary to obtain room temperature electroluminescence [4].

After implantation (Er and O in CZ-Si, $1x10^{14}$ cm^{-2}/$1x10^{15}$ cm^{-2} respectively) two sets of samples – one treated by solid phase epitaxy (set 1, 600 °C/15 min. in N_2 atmosphere), the other "as implanted" (set 2) – were hydrogenated using a plasma enhanced CVD treatment for 1 hour at 260 °C. The samples were then annealed at various temperatures in the range between 450 °C to 1000 °C.

All samples of set 1 show an enhancement of the luminescence yield by at least a factor of 5 compared to similarly prepared samples without hydrogen. At temperatures higher than 700 °C the so-called "cubic Er centre", which was previously observed only in samples with low concentrations of Er and O, becomes more and more visible. It is dominant in samples annealed at 900 °C, whereas the Er-O complexes [5] that dominate without H-treatment for high Er concentrations and similar annealing conditions are not seen anymore.

Secondary Ion Mass Spectroscopy measurements give evidence for an enhanced diffusion of oxygen and erbium at this temperature towards the surface. Etching shows that the PL does stem from a deeper region with lower erbium concentration. The luminescence yield in the hydrogenated samples is significantly higher even if compared to samples prepared to optimize the cubic centre luminescence. We thus conclude that hydrogen can enhance the solubility of the cubic centre in Si:Er,O.

References:

[1] H. Ennen, J. Schneider, G. Pomrenke, A. Axmann, Appl. Phys. Lett. **43** (1983) 943

[2] S. Coffa, G. Franzo, F. Priolo, MRS Bulletin **23** (1998) 25

[3] R. Job, A. G. Ulyashin, W. R. Fahnrer, A. I. Ivanov, L. Palmetshofer, Appl.Phys. A **72** (2001) 325

[4] W. Jantsch, S. Lanzerstorfer, L. Palmetshofer, M. Stepikhova, G. Kocher and H. Preier Physica B **273-274**, (1999) 330-333

[5] H. Przbylinska, et.al. Phys.Rev.B **54** (1996) 2532

Time-Resolved Measurement of Intersubband Population Dynamics

T. Müller, W. Parz, G. Strasser, and K. Unterrainer
Institut für Festkörperelektronik, TU Wien, Floragasse 7, 1040 Wien, Austria

The large spectral width of ultrashort optical pulses makes it possible to measure the complete time-resolved absorption spectrum of a sample with a single pulse, offering simultaneously high resolution in both the time and frequency domains [1]. We have used ultrashort mid-infrared (MIR) pulses to measure the dynamic intersubband absorption spectrum of an asymmetric double quantum well excited by an ultrashort optical pulse. In our experiment an interband pump pulse injects electrons into the first and second subband of the double quantum well structure (level-spacing $E_{21} < \hbar\omega_{LO}$). The time evolution of the decay of this coherent excitation into an incoherent electron population in the two subbands and their decay is monitored by probing the MIR absorption to a third (empty) subband. The MIR probe pulse is generated by phase-matched difference-frequency mixing in a 30 µm thin GaSe crystal. The spectrum of the MIR pulse transmitted through the sample (T = 5 K) is obtained by measuring directly the electric field using a cross-correlation technique [2].

The intersubband absorption spectra of our asymmetric coupled quantum well taken at different time-delays (> 1 ps) after the pump pulse exhibit two absorption peaks. The low-energy peak is due to the (2–3) intersubband absorption, while the second peak is attributed to the (1–3) absorption. The amplitude of the first peak decreases with time-delay after excitation due to intersubband relaxation, while the amplitude of the second peak first rises slightly and subsequently it decreases due to carrier recombination. Since the area under the peak (i–3) (i = 1,2) is directly proportional to the subband population $n_i(t)$, we are able to determine the population dynamics in the quantum well on the basis of the time-resolved absorption spectra [3].

At delay-times < 1 ps after excitation the relative phase of the excited states is not yet randomized. The time-resolved intersubband absorption exhibits two contributions: (i) a steplike increase of the absorption which rises within the time resolution of the experiment and shows either a slow decay or an increase at later times, and (ii) a superimposed oscillatory signal. As already discussed, the first signal represents the time-dependent electron population in the first and second subband after excitation. The oscillatory signal (ii) is due to quantum interference: Since the bandwidth of the probe pulse is larger than the energy splitting E_{21} the field interacts with both the (1–3) and the (2–3) transition. The states 1 and 2 are coherently excited and transitions to 3 occur through two coherent paths, whose transition probability amplitudes interfere. Depending on the time-delay we observe either reduced or enhanced absorption due to destructive or constructive interference between the contributions of the two levels. Phase relaxation destroys the 1–2 coherence and the photoexcited wave-packet decays into an incoherent subband population [4].

References:

[1] R. Huber et al., Nature **414**, 286 (2001).

[2] J.N. Heyman, R. Kersting, K. Unterrainer, Appl. Phys. Lett. **72**, 644 (1998).

[3] T. Müller, R. Bratschitsch, G. Strasser, and K. Unterrainer, Appl. Phys. Lett. **79**, 2755 (2001).

[4] T. Müller, W. Parz, G. Strasser, and K. Unterrainer, submitted to Phys. Rev. Lett.

Dynamics between Electronic Levels in InAs Quantum Dots

F.F. Schrey, T. Müller, S. Anders, L. Rebohle, W. Schrenk, K. Unterrainer, and G. Strasser
Inst. für Festkörperelektronik, Technische Universität Wien, Floragasse 7, A-1040 Wien, Austria

InAs and InGaAs quantum dot (QD) ensembles embedded in GaAs matrices or GaAs quantum well structures offer remarkable properties for fast and efficient optoelectronic devices such as NIR lasers [1]. The energy spacing of electronic states coupled with efficient electron capture capabilities into these discrete states predestine dots to be used as MIR photodetectors and emitters. In contrast to subband transitions in two-dimensional structures the density of states is peaked at the transition energy, which reduces the phase space for scattering. Therefore we expect longer relaxation and dephasing rates in QDs, which makes them very suitable for optoelectronic devices and turns them into candidates for q-bit operations.

Starting with energy level engineering in QD structures for MIR-photodetectors [2], we demonstrated recently the first MIR emission of InAs-QDs in a GaAs/AlGaAs quantum cascade structure under electronic excitation [3]. A reduced dimensionality should improve the performance of quantum cascade lasers (QCL) mainly due to suppressed electron-electron scattering. Furthermore the energy level engineering led to efficient coupling between the 2-dimensional minibands in the quantum well (QW) structure and the 0-dimensional dots, opening the way for efficient electron injection and extraction for QDs.

For the design of a QD-QCL not only the value of the transition energy, but also the knowledge of the relaxation and dephasing times are important. We use ultrabroadband MIR time-domain spectroscopy to determine these times [4]. We hope to achieve coherent excitations within the electronic dot levels, which would allow very fast control of such devices.

References

[1] D. Bimberg, N. N. Ledentsov, N. Grundmann, N. Kirstaedter, O. G. Schmidt, M. H. Mao, V. M. Ustinov, A. Y. Egorof, A. E. Zhukov, P. S. Kopev, Z. I. Alferov, S. S. Ruvimov, U. Goesele, and J. Heydenreich, Phys. stat. sol. (b) **194**, 159 (1996).

[2] L. Rebohle, F.F. Schrey, S. Hofer, G. Strasser, K. Unterrainer, APL **81**, 2079 (2002).

[3] S. Anders, L. Rebohle, F.F. Schrey, W. Schrenk, K. Unterrainer and G. Strasser; *Electroluminescence of a quantum dot cascade structure*; to be published

[4] T. Müller, R. Bratschitsch, G. Strasser and K. Unterrainer; APL **79**, 2755 (2001)

Comparison of MBE Grown IV–VI Microcavity Lasers for the Mid-Infrared with Active Regions of Different Dimensionality

T. Schwarzl[1], M. Böberl[1], J. Fürst[2], W. Heiss[1], H. Pascher[2], G. Springholz[1]
[1] Institut für Halbleiter- und Festkörperphysik, Johannes Kepler Universität Linz, Altenbergerstr. 69, A-4040 Linz, Austria
[2] Experimentalphysik I, Universität Bayreuth, Universitätsstr. 30, D-95447 Bayreuth, Germany

Coherent emitters for the mid-infrared range are of high interest due to various gas absorption lines in this region allowing high-resolution gas spectroscopy. For these applications, typically edge-emitting semiconductor lasers made from lead salt (IV-VI) compounds are used permitting to access emission wavelengths as long as 30 µm at cw operation temperatures as high as 223 K. Apart from the conventional edge-emitting lasers also surface-emitting lead salt microcavity lasers were recently demonstrated [1], [2]. These microcavity lasers offer several advantages over edge emitters like small beam divergence, single mode operation, and simplified monolithic integration. For these lasers, pulsed emission at temperatures as high as 65 °C has been achieved by our group [3].

In this work, we present a comparison between IV–VI vertical-cavity surface-emitting lasers (VCSELs) containing active regions of different dimensionality but with a nearly identical optical design of the cavity. In addition, the same optical set-up as well as pump source was used for laser excitation and characterization. This allows studying the influence of the dimensionality of the active material on the laser properties. The VCSEL samples were grown by MBE on (111) oriented BaF_2 substrates and consist of high-reflectivity PbEuTe/EuTe Bragg mirrors where only three layer pairs are required for reflectivities above 99 %. This is possible due to the exceptionally high refractive index contrast between the mirror materials. The laser active regions consist either of highly-ordered PbSe/PbEuTe self-organized zero dimensional (0D) quantum dot superlattices [4], two dimensional (2D) PbTe/PbEuTe multi-quantum wells, or three dimensional (3D) bulk-like PbTe. The VCSELs were optically pumped with ns pulsed laser excitation at a wavelength of about 1.9 µm. For the 0D quantum dot active medium, laser emission is obtained between 3.5 and 4 µm at temperatures up to 150 K. The results for the lasers with 2D active regions are similar to those with the 3D bulk-like active regions, for which lasing at 4.4 µm, 3.8 µm and 3.6 µm is observed up to temperatures of 317 K. The threshold pump intensity is only 4 kW/cm^2 at 195 K, and 15.6 kW/cm^2 at room temperature [5]. These values are much smaller than those reported for III-V mid-infrared VCSELs of 235 kW/cm^2 at 260 K, as well as those reported for a bulk-like PbSe VCSELs of about 70 kW/cm^2 at T = 239 K.

References:

[1] T. Schwarzl, W. Heiss, G. Springholz, et al., Electron. Lett., 36, 322 (2000).

[2] G. Springholz, T. Schwarzl, M. Aigle, et al., Appl. Phys. Lett., 76, 1807 (2000)

[3] W. Heiss, T. Schwarzl, G. Springholz, et al., Appl. Phys. Lett., 78, 862 (2001)

[4] G. Springholz, V. Holy, M. Pinczolits and G. Bauer, Science 282, 734 (1998)

[5] J. Fürst, H. Pascher, T. Schwarzl, et al., Appl. Phys. Lett., 81, 208 (2002)

Molecular Beam Epitaxy of $PbSe_{1-x}Te_x$ for Strain Engineering in IV-VI Semiconductor Heterostructures

A. Hallbauer, T. Schwarzl, R. T. Lechner, and G. Springholz
Institut für Halbleiterphysik, Johannes Kepler Universität, A-4040 Linz, Austria

The narrow band gap IV-VI semiconductors (PbSe, PbTe, PbS) have long been used for mid-infrared optoelectronic device applications. These structures are usually grown on lattice-mismatched substrates such as BaF_2 or Si with appropriate fluoride buffer layers. In heterostructures, band structure engineering is achieved by alloying with the wide band gap Eu or Sr chalcogenides or with the tin chalcogenides for reducing the band gaps. Because these compounds exhibit a lattice-mismatch of a few percent with respect to their lead salt counterparts, the lattice constants of the ternaries significantly change with changing alloy composition. This can be compensated by admixtures of PbSe and PbTe, because the lattice constant of PbSeTe can be adjusted over a wide range due to the rather large difference of the PbSe and PbTe lattice-constants (a_{PbTe} = 6.462Å, a_{PbSe} = 6.124Å). This can be utilized not only for achieving a lattice-matching to various substrate materials, but also for strain engineering in heterostructures as well as growth of high finesse epitaxial Bragg mirrors that are used for IV-VI compound vertical cavity surface emitting laser devices.

In the present work, the growth behavior and the structural and electronic properties of $PbSe_{1-x}Te_x$ layers grown by molecular beam epitaxy onto (111) BaF_2 substrates was investigated. For this purpose a series of samples was grown at a temperature of 380 °C with ternary compositions adjusted in the range of x = 0 – 100 % by controlling the flux rates from the PbTe and PbSe effusion cells. The alloy composition was determined precisely from beam flux rate measurements performed using a quartz crystal microbalance moved into the substrate position. These measurements were calibrated using several PbSe/PbSeTe and PbTe/PbSeTe superlattices in which the layer thicknesses were precisely determined by x-ray diffraction. Thus, a relative precision of the chemical composition of better than +2% could be achieved.

All layers were characterized by high resolution x-ray diffraction, FTIR transmission and atomic force microscopy measurements. It was found that the ternary lattice constant as a function of alloy composition precisely follows the Vegards law. With respect to the energy band gap, a pronounced deviation from a linear behavior was found, with only a minor change in E_g of PbSeTe with respect to the 325 meV PbTe band gap for Se concentrations up to about 50%. Above this composition, the band gap linearly decreases to the PbSe band gap of 180 meV at 300 K. This can be explained by the fact that the character of the conduction and valence bands of PbTe and PbSe are exchanged. With respect to the refractive index only a linear dependence of n versus x_{Se} was found. A particularly interesting effect was observed concerning the structural properties and threading dislocation density as determined from an analysis of large scale AFM images. For the pure PbSe and PbTe binaries grown on lattice-mismatched BaF_2, rather low threading dislocation densities of around 10^7 cm^{-2} were observed as well as narrow x-ray rocking curve widths. With increasing alloy composition, however, both parameters drastically increase reaching a maximum for Se concentrations of ~50%. This effect is attributed to a strong alloy hardening of the layers, which prevents an efficient relaxation of the layer/substrate lattice-mismatch by glide of dislocations. Therefore, the efficient dislocation annihilation processes known, *e.g.*, for pure PbTe are kinetically suppressed in the ternary layers. On the other hand, narrow rocking curves and very low threading dislocation densities were achieved for layers lattice matched to BaF_2 (x_{Se} = 77%).

Intermixing and Shape Transitions of PbSe Quantum Dots during Overgrowth

A. Raab and G. Springholz
Inst. für Halbleiter- und Festkörperphysik, Universität Linz, A-4040 Linz, Austria

Self-assembled semiconductor quantum dots synthesized via the Stranski-Krastanow growth mode have attracted great interest due to their excellent electronic and optical properties. For applications, quantum dots have to be embedded in a matrix material to avoid surface recombination effects. However, it is well known that e.g. for InAs dots embedded in GaAs there is significant intermixing between dot and matrix material, which leads to remarkable changes in the dot size and shape for the overgrown dots. Similar effects have been also observed for SiGe dots overgrown by silicon layers, and the degree of intermixing was found to depend strongly on the growth conditions. Since the optical and electronic properties depend crucially on size and shape of the embedded dots it is important to gain detailed knowledge about the changes of these parameters due to the capping process.

In the present work we have investigated the overgrowth behavior of self-assembled PbSe quantum dots grown by molecular beam epitaxy (MBE) on PbTe (111). The PbSe dots are formed due to strain-induced coherent islanding (–5.4% lattice-mismatch) once the critical coverage of 1.5 PbSe monolayers (ML) is exceeded. The surface islands have a well defined pyramidal shape with triangular base and with (100) side facets. For the overgrowth studies a series of dot samples was prepared under identical conditions with a total PbSe thickness of 5 monolayers. Then the PbSe dots were overgrown with $Pb_{1-x}Eu_xTe$ cap material of different Eu concentration and different cap thickness. The evolution of the surface morphology was determined using *in situ* reflection high-energy electron diffraction (RHEED), as well as *ex situ* atomic force microscopy (AFM) under ambient conditions after rapid quenching of the partially capped samples to room temperature.

From the evolution of the RHEED patterns and the intensity of the 3D (224) diffraction spot as a function of cap layer thickness for several different $Pb_{1-x}Eu_xTe$ cap layer compositions, it is found that in all cases a rapid replanarisation takes place during the overgrowth process. However, the cap layer thickness required for complete surface planarization strongly increases as a function of the Eu content in the ternary cap layer. Similar results were obtained from the AFM images of the partially capped samples. From the statistical evaluation of the AFM images, the remaining PbSe island height was determined as a function of the cap thickness, where the initial average PbSe dot height of the samples before overgrowth was 105 Å as determined from reference samples. In all cases the dot height decreases essentially linearly with increasing cap thickness, the critical cap layer thickness required for planarization increases from only 30 Å for PbTe capping to about 100Å for capping with $Pb_{1-x}Eu_xTe$ with x_{Eu} = 10%. This indicates that while a very strong intermixing and dissolution of the initially 105Å high dots takes place during pure PbTe overgrowth, this effect is strongly suppressed by the presence of Eu in the cap layer, i.e., for sufficiently high Eu concentrations the dot shape is preserved during the overgrowth process.

Transient-Enhanced Surface Diffusion on Natural-Oxide-Covered Si(001) Templates during Vacuum Annealing

H. Lichtenberger[1], M. Mühlberger[1], C. Schelling[1], S. Senz[2], F. Schäffler[1]
[1] Institute of Semiconductor and Solid State Physics, Johannes Kepler University Linz, Altenbergerstraße 69, A-4040 Linz, Austria
[2] Max Planck Institute of Microstructure Physics, Weinberg 2, D-06120 Halle, Germany

Shrinking the dimensions of semiconductor devices structures to the nanometer range, the preparation and conservation of small morphological features becomes increasingly relevant. The surface free energy of a structured heterosystem is determined by composition, crystal orientation and strain. The interplay between these parameters is widely exploited for the fabrication of self-organized nanostructures. Pre-patterned substrates can enhance ordering of these sub-micron structures. Here we report on the morphological integrity of such templates under chemical and thermal treatments typically employed during device processing.

Our studies were concentrated on samples consisting of periodic wire arrays of rectangular cross section fabricated by holographic lithography and subsequent reactive ion etching on Si(001) substrates. Periods were varied between 400 – 2000 nm at etch depths of typically 250 nm. After photoresist stripping the samples underwent an RCA clean with or without a final HF-dip immediately before transfer into the UHV environment of an MBE system. Here the samples were radiatively annealed for 1 – 5 min at 900 – 950 °C, which corresponds to the standard oxide desorption step prior to epitaxial growth [1], [2]. Samples that had the natural oxide removed by HF showed no significant morphological changes. However, on all samples covered by natural oxide the originally rectangular profiles were transformed into {311}-faceted trapezoids concomitant with a loss of up to 80% of the peak-to-valley modulation. This shape transformation requires drastically enhanced mass transport, which occurs only in the presence of SiO_2 on the surface, and consequently ceases after complete oxide desorption. The observed transient effect has to be distinguished from the conventional Si-surface self-diffusion [3] and facet formation at thermal equilibrium [4]. We examined the sidewall wetting of thick SiO_2 ridges on Si(001) in the Si/SiO_2 heterosystem [5], and followed by high-resolution XTEM imaging the kinetics of faceting as a function of the annealing conditions. The results show that even proven and supposedly uncritical process steps can drastically affect the morphology of nanostructures.

References

[1] E. Kasper, M. Bauer, and M. Oehme, Thin Solid Films **321** (1998), 148

[2] E. A. Gulbransen and S. A. Jansson, Oxid. Metals **4** (1972), 181

[3] M. E. Keeffe, C. C. Umbach, and J. M. Blakely, J. Phys. Chem. Solids **55** (1994), 965

[4] J. M. Bermond, J. J. Metois, X. Egea, and F. Floret, Surf. Sci. **330** (1995), 105

[5] Y. Zhuang, C. Schelling, J. Stangl, C. Penn, S. Senz, F. Schäffler, T. Roch, A. Daniel, J. Grenzer, U. Pietsch, and G. Bauer, Thin Solid Films **369** (2000), 409

Corresponding author: Herbert Lichtenberger, Institut für Halbleiter- und Festkörperphysik, Johannes Kepler Universität Linz, Altenbergerstraße 69, A-4040 Linz, Austria,
Phone: +43 732 2468 9602, Fax: +43 732 2468 8650.

Growth Instabilities in Si/SiGe Homo- and Heteroepitaxy

M. Mühlberger, C. Schelling, G. Springholz, F. Schäffler
Inst. für Halbleiter- u. Festkörperphysik, Johannes Kepler University Linz

J. Mysliveček, B. Voigtländer
Institut für Schichten und Grenzflächen ISG 3, Forschungszentrum Jülich, Germany

P. Šmiauer
Czech Academy of Sciences, Praha, Czech Republic

J. Krug
Fachbereich Physik, Universität Essen, Germany

The step-bunching growth instability on vicinal Si(001) in single $Si_{1-x}Ge_x$ layers and Si/SiGe superlattices was often believed to be strain-induced [1].

We show that for a large set of parameters this can be excluded with high probability and that the reason for ripple formation in the Si/SiGe system is only the kinetic step-bunching instability [2] found in Si homoepitaxy.

Single $Si_{1-x}Ge_x$ layers (with x around 0.5) do not show step-bunching. They disintegrate into hut-clusters when allowed to reach thermodynamic equilibrium [3].

In superlattices the instability has a similar behavior as the instability in homoepitaxy. Mainly the growth temperature influences the surface morphology; only little changes can be found when the germanium content in the superlattices is changed. Also the increase of ripple height and period with increasing amount of deposited silicon is similar to the one found in homoepitaxy. The more germanium is present in the superlattice the less pronounced the step-bunches appear. We attribute this decrease with increasing germanium content to changes in surface kinetics, which are due to the segregation of germanium [4].

In kinetic Monte-Carlo simulations we show that only the interplay between diffusion anisotropy on the (2×1) reconstructed Si(001) surface and the attachment/detachment of adatoms on the step-edges is responsible for the growth instability in Si homoepitaxy [5].

References:

[1] J. Tersoff, Y.H. Phang, Z. Zhang, M.G. Lagally, Phys. Rev. Lett. **75**, 2730 (1995)

[2] C. Schelling, G. Springholz, F. Schäffler, Phys. Rev. Lett. **83**, 995 (1999)

[3] C. Schelling, M. Mühlberger, G. Sprigholz, F Schäffler, Phys. Rev. B **64**, 041301R (2001)

[4] M. Mühlberger, C. Schelling, G. Springholz, F. Schäffler, Surface Science, in print (2003)

[5] J. Mysliveček, C. Schelling, F. Schäffler, G. Springholz, P. Šmilauer, J. Krug, B. Voigtländer, Surface Science **520**, 193 (2002)

High-Mobility Strained Si for Spintronics Applications

M. Mühlberger, H. Malissa, N. Sandersfeld, W. Jantsch and F. Schäffler
Inst. für Halbleiter- u. Festkörperphysik, Johannes Kepler University Linz

A. Tyryshkin and S. Lyon
Electrical Engineering Department, Princeton University, NJ, USA

Electrons in silicon are very promising for spintronics and quantum information processing. The main reasons are the extremely long spin lifetimes, which are due to silicon's weak spin-orbit coupling, and the suitability of this material system for very large scale integration (VLSI). Especially the spin properties of two-dimensional electron gases (2DEGs) in the Si/SiGe heterosystem have attracted considerable interest recently [1].

We have grown modulation-doped $Si_{1-x}Ge_x$ quantum wells ($0 \leq x \leq 0.1$) on relaxed $Si_{1-xs}Ge_{xs}$ buffer layers with $0.20 < x_s < 0.3$, and have investigated this system using conduction electron spin resonance (CESR) and conventional Hall-measurements. Growth was performed by MBE, doping with Sb was done at low temperatures (300 °C) to suppress the strong segregation. On top of a relaxed buffer layer (3.4 µm linear grading +0.6 µm constant composition part) the strained $Si_{1-x}Ge_x$ channel was deposited, followed by an undoped spacer layer, the doping layer and $Si_{1-x}Ge_x$ and Si cap layers.

For a pure Si channel mobilities of up to 341 000 cm²/Vs at carrier densities of $2.8 \cdot 10^{11}$ cm^{-2} were found in Hall-measurements under illumination at 1.6 K. In CESR extremely narrow apparent linewidths of down to 40 mG can be observed. In pulsed-ESR experiments in a comparable sample [2] it was found that the spin-lifetime T_1 (longitudinal relaxation time) and the phase memory time T_2 (transverse time) are both in the order of microseconds [3]. This is two orders of magnitude longer than the length of the microwave pulses used to flip the spins. Consequently that many coherent spin operations are possible.

The g-factor for the electrons in Si (g = 1.998) and Ge (g = 1.563) is significantly different. Since for a quantum computer [4] it would be useful to change the g-factor and therefore the position of the resonance in a CESR experiment, we grew samples with $Si_{1-x}Ge_x$ quantum wells for the electrons with x = 0.05 and x = 0.1. In these samples a clear shift of the g-factor could be observed although in this first attempt the linewidth of the CESR signal was significantly increased.

We have demonstrated the growth of high mobility modulation-doped Si quantum wells with spin lifetimes in the range of microseconds. Furthermore first steps towards the manipulation of these spins have been made with promising results.

References:

[1] W. Jantsch, Z. Wilamowki, N. Sandersfeld, M. Mühlberger and F. Schäffler, Physica E **13** (2002) 504

[2] Z. Wilamowski, N. Sandersfeld, W. Jantsch, D. Többen and F. Schäffler, Phys. Rev. Lett. **87** (2001) 026401

[3] Z. Wilamowski, W. Jantsch, N. Sandersfeld, M. Mühlberger, F. Schäffler, S. Lyon, Physica E, in print

[4] R. Vrijen, E. Yablonovitch, K. Wang, H. W. Jiang, A. Balandin, V. Roychowdhury, T. Mor and D. DiVincenzo, Phys. Rev. A **62** (2000) 012306

Laterally Ordered Ge Islands on the Pre-Patterned Si (001) Substrates

Zhenyang Zhong, A. Halilovic, F. Schäffler, G. Bauer
Institute for Semiconductor Physics, Johannes Kepler University Linz, Austria

For any conceivable application of Ge islands in electronic devices, apart from a sufficiently high size homogeneity, long range ordering is essential. In order to address individual islands, a two-dimensionally periodic alignment is required. So far several attempts for achieving this goal relied on growth through SiO_2 windows on prepatterned substrates or on Si mesas using gas source or solid source MBE. Furthermore arrays of islands grown by liquid phase epitaxy were reported.

We report on the growth of Ge rich islands on the pre-patterned Si (001) substrates by solid source molecular beam epitaxy at 680 °C or 700 °C using a Riber SIVA 45. The rather high substrate temperatures were chosen in order to enhance adatom diffusion. The pre-patterned substrates are fabricated by holographic lithography and reactive ion etching. The orientation of the stripes and the square pattern is always along <110> directions. A general growth processes are composed of a Si buffer layer and a subsequent Ge layer of 7 monolayers (MLs) or 6 MLs. Surface morphologies of some samples are shown in Fig. 1. We observe long range one-dimensional ordering of dome-shaped islands in the trenches and *not* on the ridges. In addition, the two-dimensionally ordered Ge islands nucleate in the "holes" formed by the orthogonal trenches. We attribute our observations to the importance of growth kinetics which primarily affect the preferential positioning of Ge islands on the pre-patterned Si substrates.

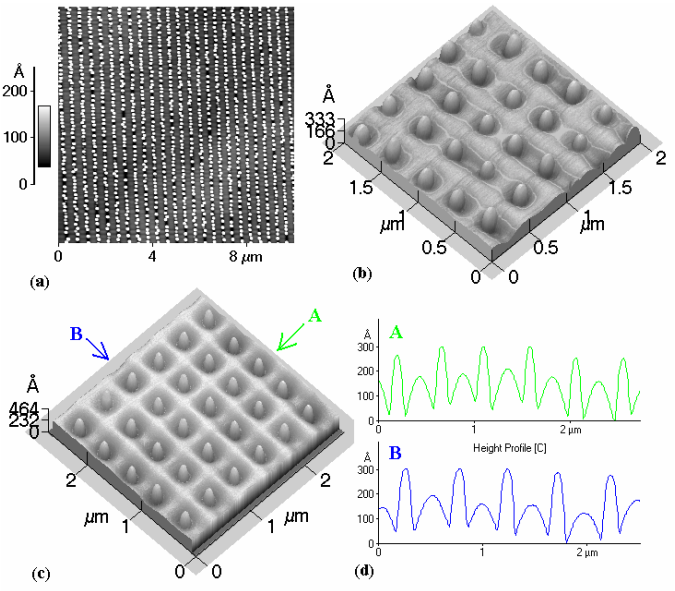

Fig. 1 (a) 2D AFM image of Ge islands on a stripe patterned substrate, (b) and (c) 3D AFM images of Ge islands on 2D hole-patterned substrates, (d) height profiles along the directions indicated by green and blue arrows in (c).

Focused Ion Beam Induced Damage in Silicon Investigated with Scanning Capacitance Microscopy

W. Brezna, H. Wanzenböck, A. Lugstein, E. Bertagnolli, E. Gornik, J. Smoliner
Inst. für Festkörperelektronik & Mikrostrukturzentrum, A-1040 Wien

Focused ion beam (FIB) techniques are among the most important tools for modification tasks below 100 nanometer. Today, FIB systems are mainly used for device modification, transmission electron microscopy (TEM) sample preparation, scanning probe microscopy (SPM) tip preparation and deposition of different metals and insulators. Unfortunately, there are mainly two effects that limit the usage of FIB modification to certain applications and areal scales. Difficult to measure, the ion beam diameter and intensity profile defines the lateral resolution and the smallest possible size of a FIB made structure. The other limitation occurs due to ion beam induced damage which extends far below the modified sample surface.

Various methods such as secondary ion mass spectroscopy (SIMS) and transmission electron microscopy (TEM) have been utilized to measure penetration depths and intensity profiles of FIBs. However, the disadvantage of these methods is their lack of 2D spatial resolution (SIMS) or difficult sample preparation (TEM). For this reason, scanning probe techniques have successfully been applied for FIB intensity profile determination and imaging in other ion beam applications. However, severe degradation of the *electronic* properties will occur long before the *structural* changes (amorphization) take place, which can not be investigated anymore with topographic AFM. In this article we introduce Scanning Capacitance Microscopy (SCM) as a very sensitive tool to investigate the position and extent of FIB induced electronic degradation. SCM can detect magnitudes smaller changes in material composition than any other scanning probe method (excluding STM) and it is possible to sense as small quantities as 10 – 100 impurity atoms per cubic micron (10^{13} – 10^{14} per cm^3). First we use this method to determine the ion beam radius and its dose dependence by investigating FIB made implantation spots. Then we will deal with the damage spread inside a FIB irradiated silicon sample.

For measuring the beam intensity profile we used the very clean surfaces of freshly cleaved silicon wafers. On the cleaved surface five types of spots were made with the FIB system, which differed from each other in the deposited ion dose (0.025, 0.05, 0.1, 0.5 and 5 pC/spot). The swelling due to the reduced density of amorphisized silicon and the subsequent silicon removal due to sputtering lead to the typical crater-like structures. Comparison of the topographic image and the SCM image shows that the damaged area is much larger than one can conclude from topography. The vast beam tails have a big impact on the sensitive SCM signal. One can define two different beam radii, one based on the topography and the other based on the SCM signal. Inside the investigated dose range the SCM based radius is always larger than the topography based radius. Where the topography shows saturation effects, the SCM based radius continues to grow with increasing ion dose. There are two reasons for this behavior. The ion beam consists of a high intensity beam center and vast beam tails that decay only very slowly. In addition the threshold dose for topographic changes and the threshold for the disappearance of the SCM signal are different. Therefore the SCM based radius can grow much more than the topography based radius when the overall ion dose is elevated. For the investigation of the ion damage below irradiated surfaces a trench was milled into the polished front side of a wafer. After milling, the sample was cleaved to get clean cross sections of the damaged area near the trench. The ion damage consists of two parts. One fraction of ions goes deep into the sample without being scattered large angles. The other fraction of ions is scattered off the beam, which leads to a reduced ion range. Therefore the damage extends about twice the distance below the valley of the trench than on the sidewalls of the trench. Previous TEM investigations of deep FIB milled polysilicon show an amorphisized region that extends about 200 nm in depth and 100 nm perpendicular. However, the damage investigated with SCM is larger by a factor of three compared to the TEM data, which is due to the high sensitivity of the SCM.

Post-Process CMOS Channel Profile Tailoring with Focused Ion Beams

A. Lugstein[1], W. Brezna[1], B. Goebel[2], L. Palmetshofer[3], and E. Bertagnolli[1]
[1] Vienna University of Technology, Floragasse 7, 1040 Vienna, Austria
[2] Infineon Technologies AG Manfred von Ardenne Ring 20 Haus E
[3] Johannes Kepler Universität Linz, Altenbergerstr. 69A, 4040 Linz

Focused Ion Beam (FIB) technology has become a critical enabler of rapid prototyping production, helping to get new IC devices to market faster. Especially for analog and mixed-signal ICs, the synergy of FIB and mechanical microprobing results in a shortening and a simplification of the debug process. Thereby the FIB is used to expose buried tracks for e-beam or mechanical probing, and to cut tracks and to make new connections which allow design modifications to be verified before new silicon is manufactured. Up to now circuit modifications are, however, restricted to the back end of the process due to FIB exposure related device degradation. Expanding FIB operations to the front end regime the unprecedented flexibility of modern FIB systems would allow for example the fabrication of transistors with different channel doping concentrations on the same die. This kind of very customized processing can be considered particularly for the fabrication of some high performance devices in limited amount on the same die, side by side with devices fabricated by conventional IC technology. For the first time we demonstrate the capability of focused ion beams for engineering in the front end regime. We show that by a robust protection for MOSFET, focused ion beam induced ESD degradation can be avoided and implantation induced damage can be well controlled and mitigated by a moderate RTA process. By a masked through gate implantation technique followed by a moderate annealing/activation process we have modified the threshold voltage of MOSFET on fully featured wafers whereby any unintentional change of devices nearby could be avoided. No degradation of gate oxide quality or increase in transistor parameter variations was observed.

To evaluate the feasibility of this scheme in terms of trap generation and damage, charge pumping was used to determine the interface state density and the residual damage after through-gate implantation and proper posttreatment. As theoretically predicted the I_{on}/I_{off} ratio of MOS devices was greatly improved by the introduction of peaking channel dopings. These devices are much less prone to hot carrier degradation due to reduced electric fields, and furthermore, less affected by DIBL, thus being easier to scale into the ultra deep submicron regime.

Deposition Mechanism of Direct-write Processes — An Application-oriented Approach to Custom-Tailored Material Properties

H.D. Wanzenboeck, S. Harasek, E. Bertagnolli
Vienna University of Technology, Floragasse 7, 1040 Vienna, Austria

Chemical vapor deposition (CVD) utilizes the adsorption and decomposition of a volatile gaseous species on a sample surface. For coating of large areas thermal CVD or plasma enhanced CVD has been established as versatile deposition technique for dielectrics and metals. In contrast to large area coating techniques a local direct-write technique is introduced using a focused energetic beam to provide the necessary activation energy for CVD. With a focused ion beam material has been locally deposited within a strictly confined area down to the nanometer range. For this direct-write nanodeposition of silicon oxide two precursor gases — siloxane and oxygen — have to be added simultaneously. For this local CVD process an exposure by a scanning beam (FIB) followed by a waiting time allowing for new re-adsorption of the precursor is required. An influence of the different ion exposure times per scan and an effect of the mixture ratio of precursors in the gas phase have been observed. The chemical composition of the solid silicon oxide and the physical properties can be tailored to demand by deliberate changes of process parameters. The beneficial aspects of the process versatility are demonstrated by deposition of insulating layers, structures with smooth surfaces and 3-dimensional structures.

Zirconium Dioxide Thin Films for Microelectronics Deposited by Metal Organic Chemical Vapor Deposition

S. Harasek, H.D. Wanzenböck, B. Basnar, J. Smoliner, and E. Bertagnolli, Institute of Solid State Electronics, University of Technology Vienna, Floragasse 7, A-1040 Vienna, Austria

The future advances in CMOS technology are to a very high degree dependent on the feasibility of further device scaling. Among the various issues in this research field, scaling of the gate dielectric is a point of special interest. This is most likely due to the fact that the forthcoming inevitable replacement of silicon dioxide rocks the foundations of today's CMOS technology. Not only a material must be identified as successor of silicon dioxide but also a new methodology for the formation of the dielectric layer has to be incorporated into the CMOS production process. As far as the material is concerned, Zirconium dioxide is among the most promising candidates. In the field of potential deposition processes various types of chemical vapor deposition (CVD) are increasingly attracting interest because of the unmatched scope of this methodology in the combination of processing at a low thermal budget and advanced performance in large-scale production. We report on a straightforward metal-organic chemical vapor deposition (MOCVD) of ultrathin zirconium dioxide using a single-source precursor system. Zirconiumtrifluoroacetylacetonate has been used as precursor material. Temperatures are kept to a maximum of 650 °C throughout the process to keep the thermal budget low. The evolution of surface topography and the dependence of the chemical composition on processing parameters are discussed as well as the electrical characteristics of the material. Electrical characterization by means of MOS structures has been performed to assess the interface quality and the dielectric properties of the layers. Interface trap density is observed to be around 5.10^{11} $cm^{-2}.eV^{-1}$ at midgap for (100)-oriented substrates and layer thicknesses down to an EOT of about 2 nm. Leakage currents in the ultrathin regime are several orders of magnitude lower than those found in equivalent SiO_2-layers.

Transport through Wannier-Stark States in Biased Finite Superlattices

M. Kast, C. Pacher, G. Strasser, E. Gornik
Institut für Festkörperelektronik, TU Wien, Floragasse 7, 1040 Wien, Austria

In semiconductor superlattices, the strong coupling of the electronic eigenstates of adjacent wells leads to the formation of minibands which are separated by minigaps. In superlattices with a finite number N of periods, each single miniband is formed by N eigenstates which are delocalized over the whole superlattice length. Applying an external electric field perpendicular to the layer planes alters the quantum mechanical confinement between the neighboring wells and leads to a splitting and a localization of the states which are then given by the Wannier-Stark states. Due to these localization phenomena the transmission channels for resonant tunneling through the miniband of the superlattice are quenched and as a consequence, electron transport through the miniband vanishes. Therefore investigations on Wannier-Stark states in semiconductor superlattices were mainly done using optical measurement techniques [1], [2].

Studying transport in biased finite superlattices requires overcoming the electric field induced decrease of resonant tunneling through the Wannier-Stark states. In this work this is achieved by the use of LO phonon scattering which can induce transitions between localized weakly overlapping states. For this purpose two different superlattices have been designed. The first superlattice consists of 5 periods of 3.5 nm $Al_{0.3}Ga_{0.7}As$ barriers and 3 nm GaAs wells, the second superlattice consists of 4 periods of 4 nm $Al_{0.3}Ga_{0.7}As$ barriers and 3.2 nm GaAs wells. The miniband width of the 5 period SL equals the optical phonon energy (36 meV) whereas the miniband width of the 4 period SL (23 meV) is well below the optical phonon energy. For this superlattice LO-phonon assisted transport through the miniband sets in at electric fields where the Wannier-Stark splitting tunes into the optical phonon energy.

A hot electron transistor [3] – [5] is used to investigate electron transport through the first minibands of the superlattices. The transmittance of the superlattice can be measured directly at given superlattice bias V_c by tuning the energy of the injected electron beam generated at the tunneling emitter barrier. The main characteristic thereby is the static transfer ratio $\alpha = I_c/I_e$ which directly reflects the probability of a hot electron to be transmitted through the superlattice. Due to the high resolution [4] of the spectrometer we are able to observe the energy splitting and the transmission behavior of the individual Wannier-Stark states separately in transport for both superlattices. The basic transport through Wannier-Stark states is identified to be coherent, the amplitudes of the quantum mechanical transmission are directly observed. Individual transport channels induced by LO-phonon scattering are observed when the Wannier-Stark states spacing tunes into the optical phonon energy.

References:

[1] E. E. Mendez et al., Phys.Rev.Lett. **60**, 2426 (1988).

[2] P. Voisin and J. Bleuse, Phys. Rev. Lett. **61**, 1639 (1988)

[3] C. Rauch et al., Phys. Rev. Lett. **81**, 3495 (1998)

[4] M. Kast, C. Pacher, G. Strasser, E. Gornik, Appl. Phys. Lett. **78**, 3639 (2001)

[5] M. Kast, C. Pacher, G. Strasser, W. S. M. Werner, E. Gornik, Phys. Rev. Lett. **89**, 136803 (2002)

Simulated and Measured Characteristic of a Micromachined Cantilever Sensor

F. Keplinger, S. Kvasnica, H. Hauser, and F. Kohl
Institute of Industrial Electronics and Material Science
Vienna University of Technology, Austria

The bending of a U-shaped Si-cantilever is used as actuator principle for measuring the magnetic fields. The deformation is caused by the Lorentz force on an electrical lead which is placed on top of the cantilever structure (Fig. 1).

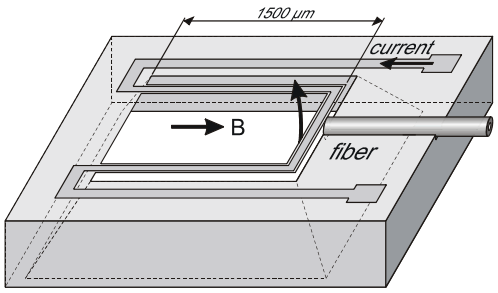

Fig. 1: Schematic drawing of the micro machined sensor for flux density with an optical readout of the cantilever position.

To find the optimal position of the fiber with respect to the cantilever in z-direction (depth of the channel for holding the fiber) the optical sensor characteristic has been estimated. For the calculations the mirror plane of the cantilever was replaced by a non transparent screen with a slit width equal to the cantilever thickness. The fiber is virtually split up into an emitting fiber and a capturing fiber which is the mirror image of the emitting one. For each point (grid) of the capturing fiber the amount of light emitted by each point of the emitting fiber is added up, considering that the rays can pass the slit, assuming a Gaussian distribution of the emitted light in the near field and that rays of the emitted and captured light lie within the acceptance angle of 23° corresponding to the fiber's numerical aperture of 0.2. Performing this procedure for each cantilever position (= shifting the gap) we get the modeled sensor characteristic.

To get a measured characteristic of the combination cantilever and optical readout the silicon was attached to the membrane of a loudspeaker and actuated at a frequency of 500 Hz. With a micro manipulator the position of the fiber in respect to the cantilever has been varied. The estimated characteristic is nearly perfectly fitted by the simulated one.

The nonlinear characteristic is caused by the changing segment size of the fiber which faces the cantilever and of the light distribution which is approximately Gaussian.

To get a higher signal to noise ratio cantilever sensors are usually excited with an ac-current producing a cantilever oscillation. Considering the offset of a real device between the center of the fiber and the zero position of the cantilever we performed simulations to predict the signal forms of the intensity.

Novel Flow-Cell to Create a Sheath Flow with Adaptable Sample Flow Dimensions

J.H. Nieuwenhuis[1], J. Bastemeijer[2], P.M. Sarro[2], M.J. Vellekoop[1]
[1] Institute of Industrial Electronics and Material Science, Vienna University of Technology, Austria
[2] DIMES, Delft University of Technology, The Netherlands

In this paper an integrated flow-cell is presented in which both the horizontal and vertical dimensions of the sample flow can be controlled dynamically. The sheath flow applied here is non-coaxial: in this device the sample flow remains in contact with one side of the channel, which assures a good contact with any sensor interface located on the channel bottom.

The sheath flow is formed by injecting the sample liquid vertically into the channel through which the sheath liquid is flowing; this forms a hydro-dynamically focused sample flow that still contacts the bottom of the flow channel. The vertical control of sample flow dimensions is achieved by controlling the relative flow-rate at which the sample liquid is injected into the sheath flow. At higher relative flow-rates the sample liquid penetrates further into the sheath liquid thereby increasing the sample flow height.

The horizontal sample flow control is achieved by adding or removing liquid through two control inlets, located on both sides of the flow-channel just down-stream of the sample inlet. When sheath liquid is added through these inlets the flow present inside the channel is compressed in the horizontal plane thereby decreasing the horizontal sample flow dimensions; when liquid is removed from these inlets the sample flow gets wider (see figure 1).

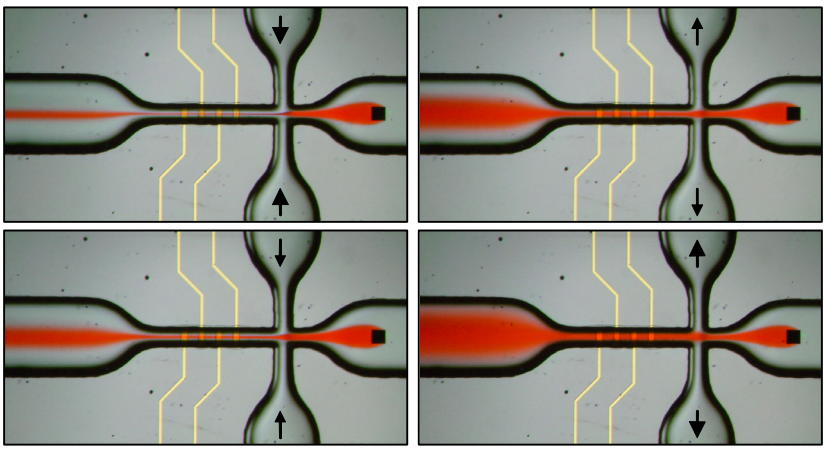

Fig. 1: Experimental results of using the control inlets to vary the horizontal dimensions of the sample flow (red color)

Micromachined Mixing Device for FTIR-Spectroscopy

P. Svasek[1], E. Svasek[1], M. Vellekoop[2], P. Hinsmann[3], B. Lendl[3]
[1] Ludwig Boltzmann Institute of Biomedical Microtechnology, Vienna
[2] Institute of Industrial Electronics and Material Science, Vienna University of Technology
[3] Institute of Chemical Technology and Analytics, Vienna University of Technology

The micromixer described here is used for the investigation of biochemical reactions by time resolved FTIR-spectroscopy. The mixing is performed *in situ*, i.e., the IR-beam directly passes the mixing chamber. It is generally known that mixing in microfluidic systems is achieved by diffusion only because of the absence of turbulent flow. Therefore diffusion distances have to be short, especially if fast mixing is required. The optical pathlenght should be short as well because of the high IR-absorption of water.

The micromixer is Y-shaped and has two inlet channels and one outlet channel, each 1 mm wide and 10 µm high. The two liquids to be mixed pass the input channels, and inside the mixing chamber they form a stack of two sheets, each 5 µm high and 1 mm wide. The mixing time is approx. 50 ms for aqueous solutions. As the injection of the two liquids is done with a high flow rate by means of a double syringe pump, there is virtually no mixing until the flow is stopped. From this moment on the mixing by diffusion takes place, the reaction starts, and a series of spectra is obtained which shows the progress of the reaction.

For the production of the device a 3-layer process has been developed that combines two 4 µm thick polymer layers (SU-8 photoresist) and one 2 µm thick metal layer in between them. This metal layer (Ag) is used to separate the two reactants until they join directly in the mixing chamber (Fig. 1). As a substrate material we use calcium fluoride because of its very high transmittance in the mid-IR range. The devices are fabricated in a batch process on 4" wafers. After patterning of the polymer and metal layers and waferbonding each waferstack contains 56 micromixers.

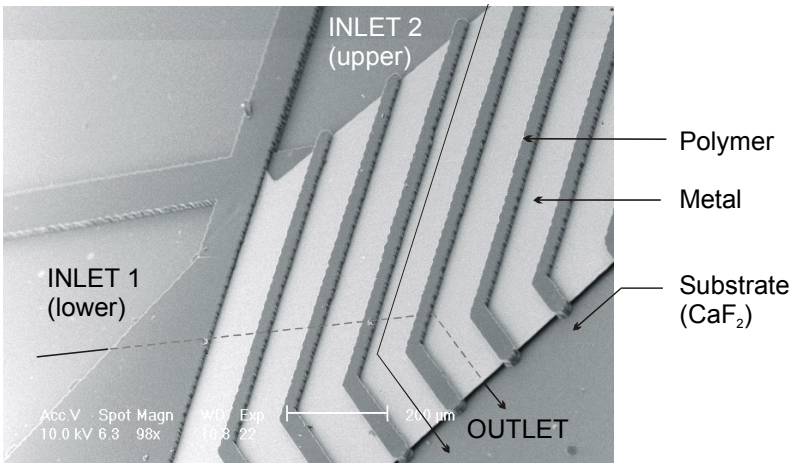

Fig. 1: SEM-Micrograph of the mixing device (shown without upper substrate)